How Halogenation Impacts the Polymer Backbone Conformation: Learning from Combination of Solid-state MAS NMR and X-Ray Scattering

Théodore Olla, Ribal Jabbour, Amina Labiod, Olivier Boyron, Stéphane Méry, Benoit Heinrich, Thomas Heiser, Denis Jacquemin, Patrick Lévêque, Anne Lesage, et al.

How Halogenation Impacts the Polymer Backbone Conformation: Learning from Combination of Solid-state MAS NMR and X-Ray Scattering

Théodore Olla[1], Ribal Jabbour[2], Amina Labiod[3], Olivier Boyron[4], Stéphane Méry[5], Benoit Heinrich[5], Thomas Heiser[3], Denis Jacquemin[6], Patrick Lévêque[3], Anne Lesage[2] and Nicolas Leclerc[1*]

(1) Université de Strasbourg, CNRS, ICPEES UMR 7515, F-67087 Strasbourg, France
(2) Centre de RMN à Hauts Champs de Lyon CRMN, FRE 2034, CNRS, Université de Lyon, ENS Lyon, UCB Lyon 1, F-69100 Villeurbanne, France
(3) Laboratoire des sciences de l'ingénieur, de l'informatique et de l'imagerie (ICube), Université de Strasbourg, CNRS, Strasbourg, F-67037, France
(4) Université de Lyon 1, CPE Lyon, CNRS UMR 5265, Laboratoire de Chimie Catalyse Polymères et Procédés (C2P2), F-69616 Villeurbanne, France
(5) Université de Strasbourg, CNRS, IPCMS UMR 7504, F-67034 Strasbourg, France
(6) Université de Nantes, CEISAM UMR 6230, CNRS, F-44000 Nantes, France

Corresponding author:

Nicolas Leclerc: leclercn@unistra.fr

Abstract

Over the last decade, halogenated semiconducting polymers have attracted considerable interest due to their outstanding optoelectronic properties. Thus, most today's OPV benchmark organic semiconductors are halogenated materials, either electron donor polymers or non-fullerene acceptor (NFA) small molecules. However, the nature and position of the substituted halogen atoms in halogenated semiconducting polymers impact, through self-assembly modification, on their optoelectronic properties in a way which is

difficult to predict. Yet, the solid-state self-assembling of this materials has been shown to be a key parameter towards high charge transport properties and photovoltaic efficiencies. In this context, there is still a need to develop analytical methods that will enable an atomic-scale structural characterization of these materials as function of the halogenation. In this manuscript, we explore the solid-state nuclear magnetic resonance (NMR) under magic angle spinning (MAS) as a tool to investigate the local structure and supramolecular organization of a series of conjugated polymers, specially designed for this study. Through a comprehensive study using complementary techniques including MAS-NMR, small and wide-angle X-ray scattering (SWAXS) and molecular modelling investigations, we have definitely succeeded in determining the molecular conformation of these polymers in relation to their chemical composition.

Introduction

Over the last decade, halogenated semiconducting polymers have attracted considerable interest due to their outstanding optoelectronic properties. Indeed, it has been recently shown that many benefits could be obtained from halogenation of conjugated materials, mainly by using fluorine and chlorine atoms,[1,2] but also bromine.[3] Because of their high electronegativity, the halogen atoms induce i) a stabilization of both the highest occupied molecular orbital (HOMO) and lowest unoccupied molecular (LUMO) levels;[4-6] ii) an enhancement of the intramolecular charge transfer (ICT) effect in alternated donor-acceptor (D-A) materials,[7] reducing consequently the bandgap of the materials; iii) the occurrence of many weak intramolecular interactions with either chalcogen atoms, other halogen atoms (halogen bonds)[8] or even hydrogen atoms (hydrogen bonds)[9] that cause geometrical constraints resulting in specific conjugated backbone conformations and/or higher backbone planarity.[10-13] These weak halogen heteroatom interactions are not only limited to the intramolecular level but may also spread out to the neighboring (macro-)molecules, leading to shorter intermolecular π-π stacking distances as well as to stronger molecular orbital overlaps and consequently to significantly enhanced charge transport properties.[14,15]

Altogether, these features make halogenated materials promising candidates for many organic electronic applications. They are thus extensively investigated in high-performance organic field effect transistors (OFET)[16] or organic photovoltaic devices (OPV).[1,17,18] For the latter devices, the deep HOMO energy level of halogenated semiconductors, used as the

electron-donor component of the photoactive layer, increases the solar cell open-circuit voltage (V_{oc}). Simultaneously, the enhancement of charge transport properties in halogenated semiconductors often benefits to the short-circuit current density (J_{sc}). Consequently, most today's OPV benchmark organic semiconductors are halogenated materials, either electron donor polymers[19-21] or non-fullerene acceptor (NFA) small molecules.[22-25]

However, the nature and position of the substituted halogen atoms as well as the chemical nature of the surrounding aromatic units in halogenated semiconducting polymers impact, through self-assembly modification, their optoelectronic properties in a way which is difficult to forecast. In this context, there is still a need to develop analytical methods that will enable an atomic-scale structural characterization of these materials as function of the halogenation. This approach is essential in order to design in a rational way halogenated materials with improved performances.

Conjugated polymers for functional material applications involve alkyl or other flexible side-chains for solubility and processability of the material but also for the control of the supramolecular packing through the formation of soft matter states and in particular mesophases. The structure can then be accessed by small and wide-angle X-ray scattering (SWAXS) for the bulk material,[26] or by grazing incidence wide-angle X-ray scattering (GIWAXS) for materials processed as thin films.[27] However, unlike crystalline structures with determined atomic coordinates, soft matter states are defined at the molecular scale, molecular fragment or molecular aggregate level. In case of unknown molecular conformation, X-ray scattering therefore only evidences the geometry and the symmetry of the structure but cannot explain the underlying molecular features. Combination with another method to molecular conformation is then the way to deepen the understanding of the system. Solid-state nuclear magnetic resonance (NMR) under magic angle spinning (MAS) has recently emerged as a unique analytical technique to investigate the local structure and supramolecular organization of conjugated polymers. For example, two-dimensional (2D) ^{1}H-^{1}H or ^{1}H-^{13}C correlation experiments have been used to probe the local packing in poly(3-hexylthiophene) (P3HT).[28] Proton-proton correlation experiments have also been applied together with GIWAXS measurements to characterize donor-acceptor stacking arrangements in cyclopentadithiophene–benzothiadiazole (CDT-BTZ)[29] and isoindigo-based D-A copolymers.[30] McGehee *et al*. implemented similar experiments to

examine the specific polymer:fullerene interactions and understand their arrangement as a function of the alkyl side chain position along the conjugated backbone.[31] More recently, ^{1}H, ^{13}C, and ^{19}F solid-state NMR experiments have been applied and analyzed jointly with GIWAXS data by Nguyen *et al*. to quantify the degree of order in polymer thin-films (Poly(2-methoxy-5-(2'-ethyl-hexyloxy)-1,4-phenylene vinylene): MEH-PPV and Poly([2,6'-4,8-di(5-ethylhexylthienyl)benzo[1,2-b;3,3-b]dithiophene]{3-fluoro-2[(2-ethylhexyl)carbonyl]thieno [3,4-b]thiophenediyl}): PTB7-Th).[32] In particular, they succeeded to correlate the order/disorder state in amorphous MEH-PPV and semi-crystalline PTB7-Th thin films with the density of states (DOS) width and the charge transport properties. Recently, molecular modelling and surface-enhanced NMR spectroscopy have been combined to characterize the polymer backbone group conformations and packing arrangement in high-mobility donor-acceptor copolymer thin films.[33]

In the present work, we use solid-state NMR spectroscopy in combination with powder XRD analysis and DFT modelling to investigate the influence of the nature and position of halogen atoms along the conjugated backbone of D-A alternated copolymers on the molecular chain conformation, and to establish correlations between this chain conformation and the spectroscopic and electronic properties. While NMR and XRD have been used as experimental tools to provide raw data, DFT modeling appears to be a valuable complementary tool to assist in the analysis of these data and the assignment of fluorine NMR peaks to certain conformations. To this aim, we finely designed a D-A alternated copolymer by varying both the nature and position of halogen atoms in order to modulate the type of possible weak bonds along the conjugated polymer backbone. As mentioned above, one of the main characteristics of halogen atoms is their ability to drive specific conformationally-locked polymer structures by halogen-induced weak interactions.[34,35] We therefore selected the 2,2'-dithiophene unit as support for halogen substitution. By using a pair of halogen atoms (fluorine or chlorine) substituted onto a 2,2- bithiophene unit (one per thiophene unit) at the 4,4' and 3,3' regioselective positions, four symmetrical dihalogenated-2,2'-dithiophene units were designed. This bis-halogenated dithiophene moiety should be regarded as electron donor units (Figure 1). As the electron withdrawing unit, we selected a thieno[3,4-*c*]pyrrole-4,6-dione (TPD) derivative.[36] TPD has the advantage to carry a long side-chain, which ensures solubility and promotes lamellar self-assembly. In addition, TPD

contains two different chemical sites that are prone to involve weak bonds with halogen atoms, i.e., the sulfur atom and the ketone group (highlighted in red in Figure 1).

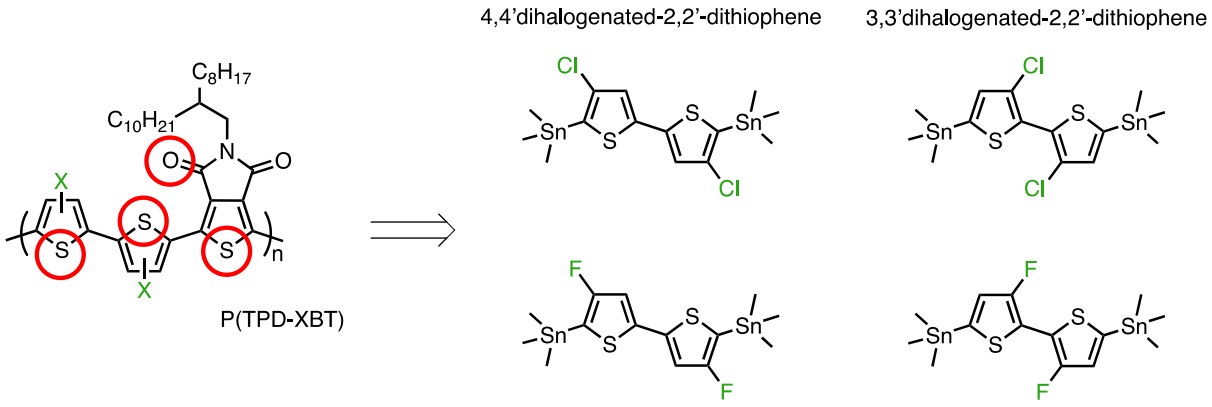

Figure 1. (left) Chemical structure of the investigated D-A alternated polymer series. The circles in red indicate the possible sites of weak bond receptors for halogens. (right) The four dihalogenated-2,2'-dithiophene units considered in this study.

By using standard characterization tools, including DFT calculations, in combination with high-resolution solid-state NMR and small and wide-angle X-ray scattering (SWAXS) on bulk polymers, we confirm that the position of halogen atoms along the 2,2'-dithiophene unit has a strong impact on the conformational structure of the repeat unit and consequently on the polymer chain self-assembly. In particular, we were able to determine the various possible conjugated backbone conformations depending on the nature and position of the halogen atom. The polymer chain self-assembly is further correlated to the charge transport properties.

Results and Discussion

Synthesis

A major effort has been devoted to the synthesis of ß-halogenated-2,2'-dithiophene. Indeed, to the best of our knowledge, the two 4,4'-dichloro-2,2'-dithiophene building blocks has never been reported so far. Moreover, the synthesis of the other dihalogeno-2,2'-dithiophene are not straightforward and deserved to be revisited and simplified. Due to the significantly differing costs of commercially available raw materials, the chemical routes towards both fluorinated and chlorinated bithiophenes differ significantly. Indeed, while it

looks reasonable to elaborate bis-ß-chlorine-2,2'-bithiophene by homocoupling of β-chlorothiophene (3-chlorothiophene is available at <10 €/g), for the fluorine derivative (about 650 €/g), it appears more appropriate to consider a post-fluorination approach of a ß,ß'-dibromine-2,2'-bithiophene precursor by electrophilic substitution (see Scheme 1).

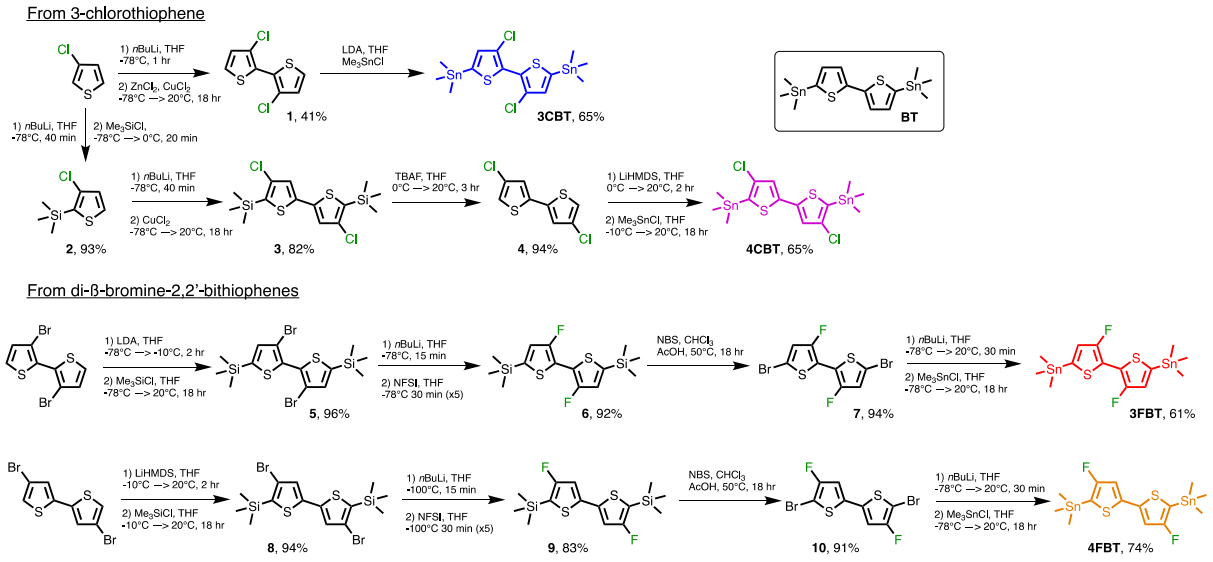

Scheme 1. Chemical routes towards ß,ß'-dihalogen-5,5'bis(trimethyltin)-2,2'-bithiophene.

The synthesis of 3,3'-dichloro-5,5'-bis(trimethyltin)-2,2'-bithiophene (compound **3CBT** in scheme 1) has been already reported.[37] The authors used a chemical route involving a selective dehalogenation of 3,3',5,5'-tetrachloro-2,2'-bithiophene to prepare 3,3'-dichloro-2,2'-bithiophene, followed by a sequence of lithiation/stannylation. It is noteworthy that the yield over the two steps was found to be < 10 %, which is likely attributed to the poor selectivity of the dichlorination step. Based on that observation, we explored two different synthetic approaches to obtain the intermediate 3,3'-dichloro-2,2'-bithiophene (compound **1**) starting from cheap 3-chlorothiophene (see Scheme S2 and details in the Supporting Information). The most straightforward one (scheme 1) consisted in an oxidative homocoupling reaction directly from 3-chlorothiophene. This coupling involved a two-step reaction with first, a deprotonation of 3-chlorothiophene in C2 position using *n*-BuLi, followed by its oxidation using a mixture of $ZnCl_2$ and $CuCl_2$. 3,3'-dichloro-2,2'-bithiophene (compound **1**) could then obtain in 41 % yield. A subsequent deprotonation/stannylation sequence allowed the preparation of **3CBT** in an overall yield exceeding 25 %.

To the best of our knowledge, the second chlorinated regioisomer, namely 4,4'-dichloro-5,5'-bis(trimethyltin)-2,2'-bithiophene (compound **4CBT** in scheme 1) has never been reported. A major difference with **3CBT** is the need for intermediate protections at C2 position in the initial 3-chlorothiophene unit (future 5- and 5'-positions in α of the chlorine atom in **4CBT**). Indeed, the presence of chlorine atom in C3 position induces a strong selectivity for electrophilic substitution in this C2 position (in α / ortho of the chlorine). The trimethylsilyl (TMS) group has been selected for its easy conversion to bromine by using NBS or deprotection by using TBAF. Here again, two routes have been explored for the synthesis of the intermediate compound **3**, the Stille cross-coupling and the oxidative homocoupling reactions. (see Scheme S3 and details in the Supporting Information). The most straightforward one (scheme 1) involved only two steps with an overall yield of more than 75 %. Then, using TBAF reagent, the TMS deprotection in compound **3** was achieved in 94 % yield. Finally, the deprotonation/stannylation sequence has been performed in 65 % yield by using LiHMDS as base, in order to be selective and to avoid chlorine substitution. The total yield of this **4CBT** synthetic route from the 3-chlorothiophene was about 45 %.

Regarding 3,3'-difluoro-5,5'-bis(trimethyltin)-2,2'-bithiophene (compound **3FBT** in scheme 1), we followed a synthetic route already reported.[38,39] Starting from 3,3'-dibromo-2,2'-bithiophene, it involved four chemical steps, including protection at C5 and C5' positions by TMS groups. The key step clearly remained the difluorination of the brominated positions. It was achieved by a lithiation with *n*-BuLi followed by a treatment with N-fluorobenzenesulfonimide (NFSI) in one-pot. However, this sequence had to be repeated five times, in one pot, to afford the compound **6** in high yield of 92 %. Keeping the temperature at -78°C was crucial as the dicarbanion specie is poorly stable in ß-positions. Then, the TMS groups in **6** could be converted to bromine atoms almost quantitatively by using a stoichiometric amount of NBS to afford compound **7**. Finally, a standard lithiation/stannylation sequence led to the synthesis of **3FBT** with an overall yield of approximately 50 %.

In this paper, we also report the synthesis of the 4,4'-difluoro-5,5'-bis(trimethyltin)-2,2'-bithiophene (compound **4FBT** in scheme 1). The selected synthetic pathway, which differs slightly from a previous report,[40] was very similar to the one used for **3FBT**, so the same reaction sequence was applied to 4,4'-dibromo-2,2'-bithiophene. Only the two first steps differed significantly in conditions. For the starting TMS protection, in particular, LDA was

replaced by LiHMDS to form complexes with bromide atoms selectively at positions 4 and 4', leading the next step to the desired 4,4'-dibromo-5,5'-bis(trimethylsilyl)-2,2'-bithiophene (compound **8**). Alternatively, compound **8** could also be directly synthesized in two steps, by starting from cheap 3-bromothiophene (Scheme S4). Here again, the second fluorination step required optimization. Indeed, at -78°C, only bithiophene degradation was observed after lithiation, showing that the 4,4'-dicarbanion specie stability is even worse than the one of its 3,3'-derivative counterpart (*see above*). By decreasing the reaction temperature to -100°C, as shown by Bura *et al*.,[14] we could successfully prepare compound **9** with a high yield of 83 %. However, probably due to the poor temperature control at -100 °C, the yield was found to be highly dependent of the quantity of starting material. The highest yields were reached from batches of 500 mg of initial compound **8**, which drastically decreased to 55 % when 1 g batch was used. Finally, after a quasi-quantitative bromination step, followed by a classical lithiation/stannylation sequence, **4FBT** was obtained with an overall yield of about 53 %.

Moreover, non-halogenated 2,2'-bithiophene has also been synthesized to be used as reference material (compound **BT** in onset in Scheme 1, see supporting information for details). All distannylated dithiophenes have been purified by several recrystallizations and characterized by ^{1}H and ^{13}C NMR, and by mass spectra analyses.

All synthesized dithiophenes have been polymerized with the 1,3-dibromo-N-alkylated TPD derivative by Stille cross-coupling.[41] Despite the long and branched alkyl side chains, the TPD-based copolymers solubilities rather low. Consequently, in order to push further the copolymerization and reach reasonably high molecular weights, a mixture of solvents was used (toluene/dimethylformamide) and the polymerization time was extended to 48 hours. Five new copolymers have then been elaborated (Scheme 2). The polymers were purified by Soxhlet extraction from which several fractions were collected and isolated. The average molar mass per number (Mn), per weight (Mw), and the dispersity (*Đ*), were measured by high-temperature size exclusion chromatography (SEC) at 150°C using 1,2,4-trichlorobenzene (TCB) as an eluent and calibrated with narrow polystyrene standards. However, the two 4,4'-ß-dihalogen-2,2'-bithiophene based polymers **P(TPD-4CBT)** and **P(TPD-4FBT)**, essentially led to insoluble fractions, i.e., not soluble enough even at high temperature in TCB, to be characterized by SEC.

For each copolymer, the highest molecular weight fraction features are summarized in Table 1. SEC profiles show monomodal distributions with no trace of residual monomers. We underline that all polymers show Mn in a similar range of about 10 to 20 kg/mol. The rather low molar masses measured are mainly due to the limited solubility of this series of polymers, which i) involves polymer precipitation during polymerization and ii) makes SEC analysis complicated with most likely aggregated particles remaining in the filter and therefore not being injected even at 150°C into the TCB. However, it is worth noting that these molar mass values are comparable to those reported in the literature for structurally equivalent polymers.[44]

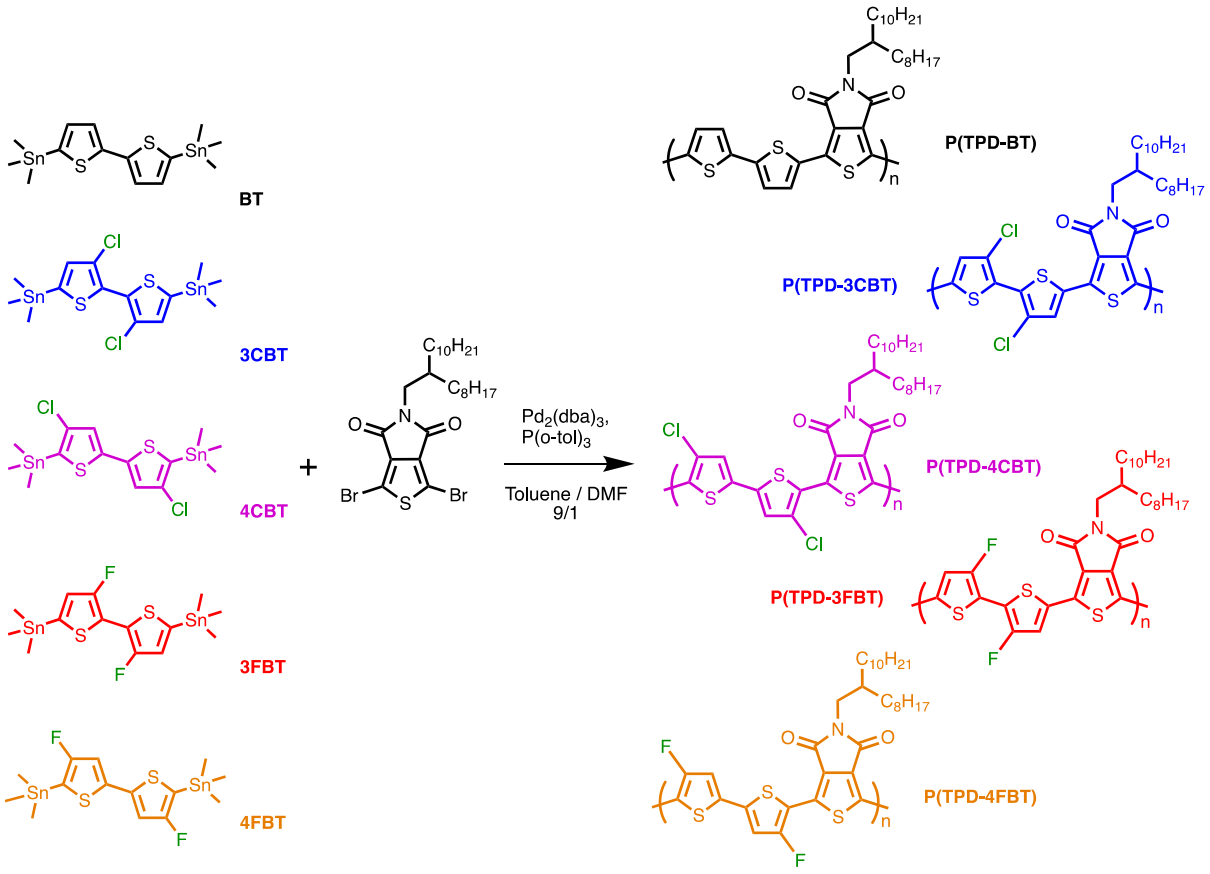

Scheme 2. Synthesis of TPD-based copolymers by Stille cross-coupling.

The polymers were also characterized by thermogravimetric analysis (TGA). All of them exhibit high thermal stability without significant weight loss below 260°C and with an observed 5% weight loss temperature (T_d) under nitrogen above 360°C (see Table 1 and Figure S5). The polymer chemical composition had little impact on the stability properties,

the halogenated polymers being somewhat less stable than the unsubstituted polymer and the chlorinated slightly less than the fluorinated.

Polarizing optical microscopy (POM) and differential scanning calorimetry (DSC) were used to investigate the thermal behavior of the polymers. At room temperature they are opaque, glassy-like solids that gradually soften above 120°C to birefringent, paste-like states (Figure S6). No textural changes are observed below 300°C, in accordance with DSC runs that do not display any phase transition (Figure S7).

Table 1. Molecular weights, decomposition temperatures along with absorption and electrochemical data of the polymers

	[Mn] ($kg.mol^{-1}$) / $Đ$	T_d (°C)[a]	Absorption			Cyclic Voltammetry[b]		
			λ_{max} solution (0-2 / 0-1 / 0-0 bands in nm)	λ_{max} film (0-2 / 0-1 / 0-0 bands in nm)	E_g opt (eV)[b]	E_{ox} (V) / HOMO (eV)	E_{red} (V) / LUMO (eV)	E_g CV (eV)
P(TPD-BT)	8.6 / 1.6	419 ± 5	533 / 585 / 642	533 / 577 / 640	1.71	0.68 / -5.42	-1.13 / -3.27	2.15
P(TPD-3CBT)	10 / 1.9	366 ± 5	530 / 573 / 631	530 / 572 / 628	1.80	1.18 / -5.58	-1.1 / -3.3	2.28
P(TPD-4CBT)	Not soluble	373 ± 5	520 / 571 / 618	522 / 576 / 615	1.86	1.31 / -5.71	-1.2 / -3.2	2.51
P(TPD-3FBT)	16 / 1.8	372 ± 5	535 / 585 / 639	536 / 581 / 641	1.77	1.08 / -5.48	-1.03 / -3.37	2.11
P(TPD-4FBT)	Not soluble	408 ± 5	520 / 570 / 619	523 / 576 / 628	1.80	1.22 / -5.62	-1.25 / -3.15	2.47

[a] T_d: 5 % weight loss temperatures measured by thermogravimetric analysis (TGA) at 5°C/min under N_2 atmosphere. [b] from thin-films

Optical and Electrochemical Properties

The low solubility, at room temperature, is a common feature of many halogenated polymers.[42] In order to probe their respective propensity to form aggregates in solution, the UV-vis absorption polymer profiles in diluted *o*DCB solutions at various temperatures were recorded (Figures S8-S12). None of the polymers showed a clear evolution of its absorption spectrum as a function of temperature. An investigation of polymer solutions by dynamic light scattering (DLS) at a concentration 5 times lower than the one used in UV-visible experiments, showed that all solutions present aggregates of about 200 nm in size at room temperature. This suggests that our polymers are not soluble enough in *o*DCB to reach

the soluble state, even at high temperature (95°C). In addition, a comparison between solution and thin-film absorption spectra point out a minor evolution between both states, suggesting the existence of aggregates in solution for all polymers.

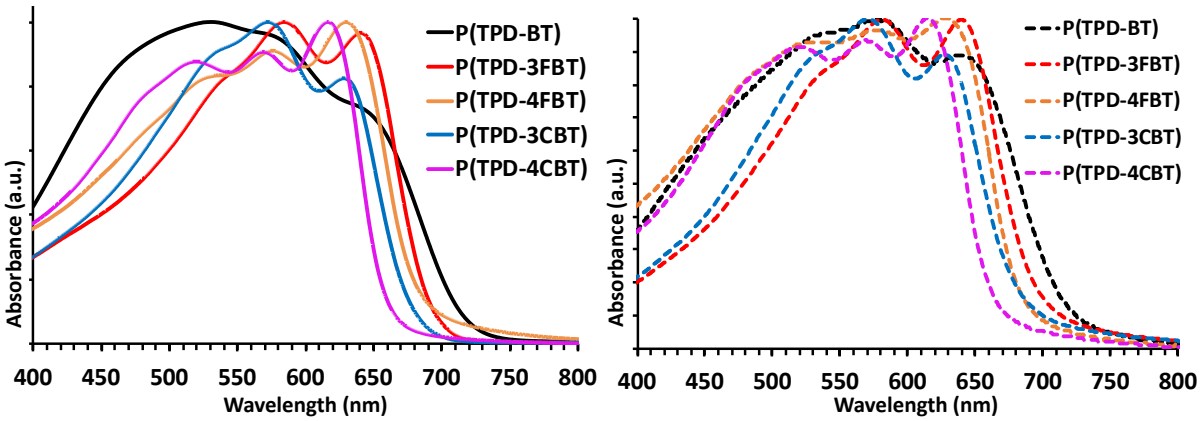

Figure 2. UV-vis absorption spectra in *o*-DCB solution (left) and in thin-film (right).

The non-halogenated reference **P(TPD-BT)** polymer exhibits the broadest and less structured band of absorption. It is nevertheless the polymer whose absorption spectrum shows the greatest evolution from solution to thin-film, with a clear increase of its vibronic structure. In solid state, its onset of absorption is the most bathochromically shifted in the series and thus, exhibits the lowest optical band gap of 1.71 eV.

Upon halogenation of polymers, a general trend is clearly observed in solution as well as in the solid state: the absorption spectra are better structured with the appearance of clearer vibronic structures essentially made up of three bands for all halogenated polymers. Among halogenated polymers, **P(TPD-3FBT)** presents the lowest band gap (1.77 eV), while **P(TPD-4CBT)** exhibits the highest one (1.86 eV).

Cyclic voltammetry has also been used to access the oxidation and reduction potentials of each polymer and to estimate HOMO and LUMO energy levels. The cyclic voltammograms are shown in Figures S10-S14, and the corresponding data along with the HOMO (E_{HOMO}) and LUMO (E_{LUMO}) energy level values are summarized in Table 1. All potentials are referred to the saturated calomel electrode that was calibrated at 0.38 V versus the Fc/Fc+ system.[43] The measured redox potentials and calculated energy levels for **P(TPD-BT)** are in good agreement with the ones reported for identical non-halogenated polymers.[44,45] As

expected, the halogenation mainly affects the oxidation potential and consequently the calculated HOMO levels.

From the first results here obtained, some trends can already be drawn on the influence of the halogen nature and position:

Influence of the halogen nature: The chlorinated polymers exhibit a clear hypsochromic shift as compared to their fluorinated counterparts (and to the non-halogenated reference) polymer, in solution as well as in solid state. Accordingly, their optical band gaps are increased of about 0.03 and 0.06 eV, for **P(TPD-3CBT)** and **P(TPD-4CBT)**, respectively. This effect is likely the signature of the higher steric hindrance of chlorine atoms, that probably disturbs the backbone planarity,[26] as confirmed below with the DFT results. In addition, chlorination is found to further decrease the HOMO levels as compared to fluorination. Such an effect of the halogen is now well established in literature. [26,46]

Influence of the halogen position: In both cases, halogenation in 3,3'-positions leads to the most bathochromically shifted absorption onsets, i.e., to the most delocalized π-electronic structure. Moreover, 4,4'-dihalogenation leads to deeper HOMO levels than 3,3'-dihalogenation.

Theoretical modelling

To provide additional insight into these compounds, first-principles calculations on the various polymers were performed using DFT and TD-DFT and modeling the environmental effects with a continuum approach (see the SI for computational details). In order to keep calculation time reasonable, we considered tetramers including two TPD units surrounding one central bithiophene unit (Figure 3). In addition, the ramified side chains were replaced by methyl groups. The impact of these two approximations was tested and found to be very mild on the relative energies, though the vertical absorption wavelengths are logically significantly bathochromically shifted in the longer models (see Tables S1 and S2 in the SI). For each polymer model, four different conformations were considered (Figure 3). Our key results, considering *o*DCB as solvent in the polarizable continuum model (PCM), are reported in Table 2. Table S3 provides the corresponding information in gas phase. As can be seen,

except for **P(TPD-3CBT),** the geometries of the various conformers in gas and condensed phases are pretty similar.

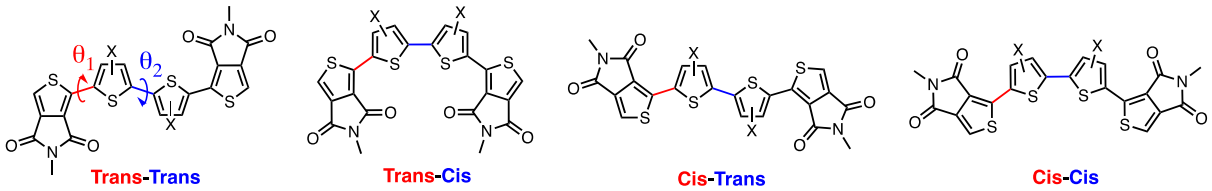

Figure 3. Representation of the different possible conformations modelled by DFT.

Table 2. Theoretical results obtained at the PCM(o-DCB)-TD-B3LYP/6-311++G(d,p)// PCM(o-DCB)-B3LYP/6-311G(d) level of theory. We report relative free energies (considering the most stable structure as reference), the key dihedral angle (in °) and the vertical excitation energy of the lowest band. Gas-phase data are given in the SI.

Isomer	Halogen	Conformation	ΔG (kcal.mol^{-1})	Φ_1	Φ_2	λ_{abs} (nm)
None	-	*Trans*- *Trans*	0.46	177.4	168.8	511
		Trans- *Cis*	1.78	179.4	17.3	510
		Cis- *Trans*	0.00	1.7	167.3	515
		Cis - *Cis*	0.86	0.4	17.9	512
3,3’	F	*Trans* - *Trans*	0.39	180.0	180.0	510
		Trans - *Cis*	2.73	177.7	37.8	481
		Cis - *Trans*	0.00	0.0	180.0	514
		Cis - *Cis*	2.12	1.3	37.8	485
	Cl	*Trans* - *Trans*	2.44	180.0	180.0	502
		Trans - *Cis*	1.49	179.7	62.6	429
		Cis - *Trans*	0.00	1.9	126.8	447
		Cis - *Cis*	1.47	2.1	62.3	433
4,4’	F	*Trans* - *Trans*	0.00	179.5	162.2	492
		Trans - *Cis*	0.05	179.7	19.4	493
		Cis - *Trans*	4.99	41.6	157.8	445
		Cis - *Cis*	5.46	41.2	28.1	438
	Cl	*Trans* - *Trans*	0.00	179.1	160.0	485
		Trans - *Cis*	1.02	179.2	23.6	482

	Cis -Trans	1.78	53.5	155.7	420
	Cis -Cis	2.03	53.7	29.1	413

Concerning the relative free energy, it appears clearly that the relative stabilities predicted by the calculations differ from one isomer to another and also to some extent according to the nature of the halogens. At this point it is worth mentioning that the typical error bar of DFT for relative energies is ca. 1—2 kcal.mol^{-1}, and that simplified models are used. It is therefore necessary to take these results with caution.

For the naked model **P(TPD-BT)** polymer, the variations in relative free energy from one conformation to the other (ΔG < 1.8 kcal.mol^{-1}) are relatively small and suggest that all 4 conformations are possible, though with probably less of the least stabilized *trans-cis* conformation. Regarding the planarity of the calculated geometries, all non-halogenated models always show coplanar TPD-thiophene units, whereas the central bithiophene is slightly out-of-plane in both *trans* (ca. 12°) and *cis* (ca. 17°) conformations.

Within the 3,3'-series, the scenario is slightly dependent on the halogen atoms. For the fluorine derivative (**P(TPD-3FBT)**), ΔG varies in larger amount (ΔG > 2.7 kcal.mol^{-1}) and more notably, the bithiophene cis conformation appears to be systematically less stable as compared to the *trans*, a natural consequence of the steric clash between the two halogens in that position inducing a ca. 38° twist of the central unit. For the chlorinated derivative (**P(TPD-3CBT)**), the most likely conformation is less obvious as three conformations lead to low ΔG values, but the twist angles when the bithiophene is in cis conformation are so large (Φ_2 >60°) that it is likely that the system can be viewed as two different units in that case. For this chlorinated derivative, it is also worth noticing that significant differences are observed between the PCM and gas phase relative energies, hinting that caution is needed for the conformation prediction.

Finally, in the 4,4'-series, the fluorinated and chlorinated derivatives behave roughly the same, with the most favorable *trans* conformation between the TPD and thiophene units. For the fluorinated derivative, this trend is clearly more pronounced. ΔG varies on a broader scale with both *trans-trans* and *trans-cis* conformations being 5 kcal.mol^{-1} more stable than the other two conformations. The same trend is true for the chlorinated derivative, despite a smaller ΔG variation. In agreement, the most planar conformations are obtained when TPD and thiophene units are in trans conformation. Cis-conformations bring much steric

hindrance, inducing significant Φ_1 (41° for F, 54° for Cl), whereas the bithiophene behaves like in the unsubstituted system.

The computed absorption wavelengths corresponding to these calculated geometries were obtained using the vertical approximation for compact molecular models, and hence cannot be directly compared to experiment. However, their evolution across the series qualitatively follows the experimental trends with a non-halogenated derivative exhibiting a slight bathochromic shift as compared to the 3,3'-derivatives. Systematically, the 4,4'-derivative is even more hypsochromically shifted as compared to the 3,3'-counterparts by ca. 10-20 nm for the most stable conformers. Finally, the chlorinated derivatives always showed the lowest λ_{max} of absorption, likely due to their less conjugated structures.

To conclude on molecular modelling, a preference of conformation can be noticed as a function of the halogen substitution. Thus, the 3,3'-difluorinated material shows a most probable *trans* conformation between the two thiophene units. The 4,4'-dihalogenated derivatives show a preferred *trans* conformation between the TPD and thiophene unit. To further understand halogenation impact on polymer features, the atomic-scale structure of the polymers was investigated by solid-state NMR and SWAXS.

Proton solid-state NMR spectroscopy

The one-dimensional (1D) proton NMR spectra of the five polymers are shown in Figure 4. They are displayed with the same color code as in Schemes 1 and 2, while the spectrum of the fully protonated polymer is shown in black as a reference.

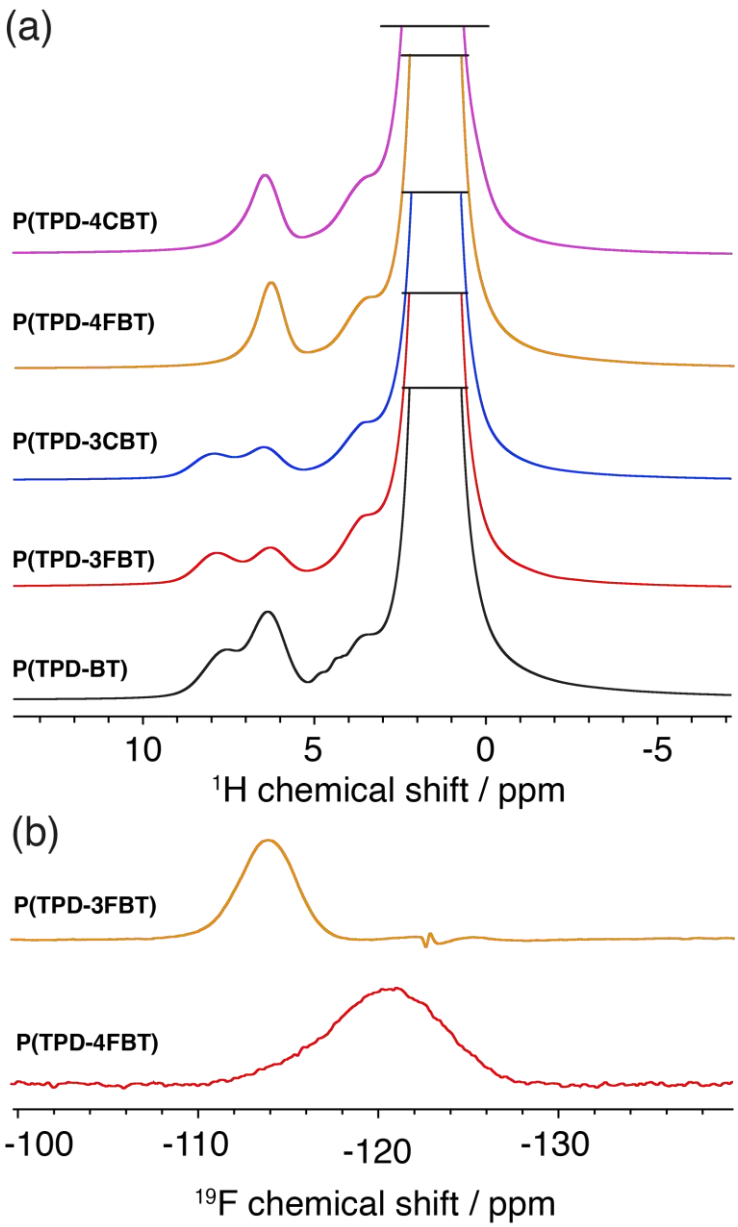

Figure 4. (a) ^{1}H MAS NMR spectra of the five conjugated polymers. Spectra were recorded at 800 MHz with a magic-angle spinning (MAS) frequency of 60 kHz. (b) ^{19}F MAS NMR spectra of the two fluorinated polymers. The color code is the same as the one used on Scheme 1.

A first overview of the ^{1}H spectra confirms that the position of the halogens is *a priori* the key factor governing the molecular structure in the solid-state of these polymers. Indeed, the NMR spectra of the halogenated polymers are identical two by two, within the 3,3'- (in red and green) and 4,4'-dihalogenated (in orange and purple) series, regardless of the nature of the halogen atom. The spectra of all four halogenated polymers exhibit a huge resonance

at around 1.6 ppm corresponding to the alkyl protons of the long side chains as well as a shoulder at 3.6 ppm assigned to the N-CH_2 methylene protons.

Both 4,4'-dihalogenated polymers, **P(TPD-4CBT)** and **P(TPD-4FBT)**, display a single aromatic resonance at ca. 6.4 ppm corresponding to the aromatic protons in 3,3'-positions of the 4,4'-dihalogenated-bithiophenes, which are both equivalents (see conformation in Figure 6a). The picture is slightly more complex for the two 3,3'-dihalogenated polymers, **P(TPD-3CBT)** and **P(TPD-3FBT)** as their proton spectra display two aromatic resonances, at around 6.4 and 7.9 ppm, in a 1 to 1 intensity distribution. This result suggests that the two hydrogens in 4,4'-positions of bithiophene are nonequivalent. This is likely related to a change in the orientation of the adjacent TPD-thiophene unit

As discussed above, two conformations can indeed be considered: a *trans* conformation where both thiophene cycles of TPD and thiophene are oriented head to toe, and a *cis* conformation where both thiophene cycles of TPD and thiophene have the same orientation (see conformations in Figure 6b). Thus, the resonance at 6.4 ppm is assigned to the *trans* conformation, and the one at 7.9 ppm to the *cis* conformation. Indeed, in such an orientation, a higher deshielding is expected due to the high electronegativity of the nearby oxygen atom, confirmed below by theoretical calculations. The integrated intensity of the two aromatic resonances is similar, indicating that both conformations coexist in an about 50/50 ratio along the conjugated backbones. For **P(TPD-3FBT)**, this result is consistent with the data of Table 2: a Boltzmann ratio would give a 66/34 ratio for *cis/trans* on the basis of DFT results, which given the approximation in the model is a very satisfying outcome. For **P(TPD-3CBT)**, theory also foresees the coexistence of *cis* and *trans* conformers, albeit in an incorrect 92/8 ratio, maybe due to the above-mentioned strong sensitivity of the conformers to the medium.

The proton spectrum of the non-halogenated polymer **P(TPD-BT)** (Figure 4, black trace) shows that both conformations are present in a cis/trans ratio of about 70/30. This calculation is made from the integrated intensity of the two aromatic resonances, assuming that the peak at 6.4 ppm corresponds to both protons in 3,3'-positions and to protons in 4,4'-positions oriented towards the sulfur atom of the TPD unit (trans conformation), while the peak at 7.9 ppm corresponds to 4,4'-positions oriented towards the oxygen (cis conformation). Here, the 70/30 ratio is compatible with the one that can be computed from a Boltzmann analysis based on the DFT free energies listed in Table 2 (71/29).

In order to further confirm our hypotheses and our demonstration, we performed the DFT calculation of chemical shifts of protons in 4,4'-positions in the previously introduced model compound consisting of two TPD units at the ends and a central *trans* bithiophene unit. The two *trans* and *cis* conformations between the TPD and bithiophene units were considered (Figure 5).

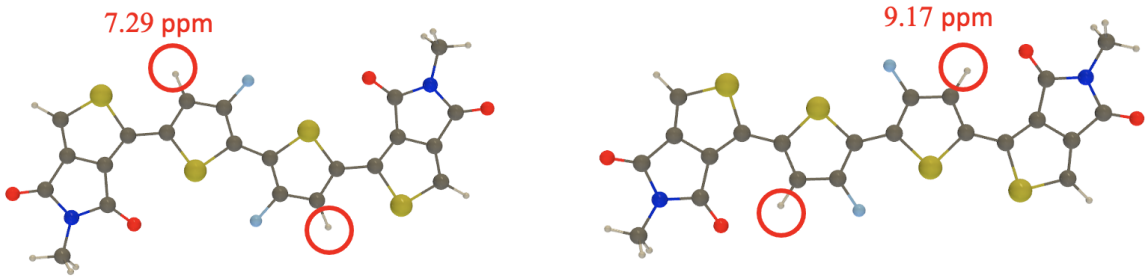

Figure 5. ^{1}H NMR calculations made on the trans-trans and cis-trans conformations of the fluorinated model.

As expected, the two conformations give rise to two distinct chemical shifts. The *cis* conformation with protons facing the TPD carboxyl group leads to a much more deshielded signal, of 9.2 ppm compared to only 7.3 ppm in the *trans* conformation. This trend is totally in line with the NMR measurements.

In order to get further insights into the relative orientation of the thiophene rings in the dithiophene unit, we implemented two-dimensional (2D) proton double-quantum (DQ) single-quantum (SQ) NMR correlation experiments. One-dimensional (1D) ^{19}F NMR spectra were also recorded for the two fluorinated polymers to obtain additional structural information (Figure 4b). In the same way as for the previously reported 1D ^{1}H NMR spectra, the 2D proton-proton correlation spectra of the polymers display the same features when halogenated in 4,4'- or 3,3'-positions, regardless of the nature of the halogen. Therefore, only the ^{1}H DQ-SQ MAS NMR spectra of the fluorinated polymers are presented herein (Figure 6). The spectra of the chlorinated materials are reported in Figure S15. Schematic structures of the conjugated backbones are represented above the 2D spectrum to facilitate the interpretation of the data.

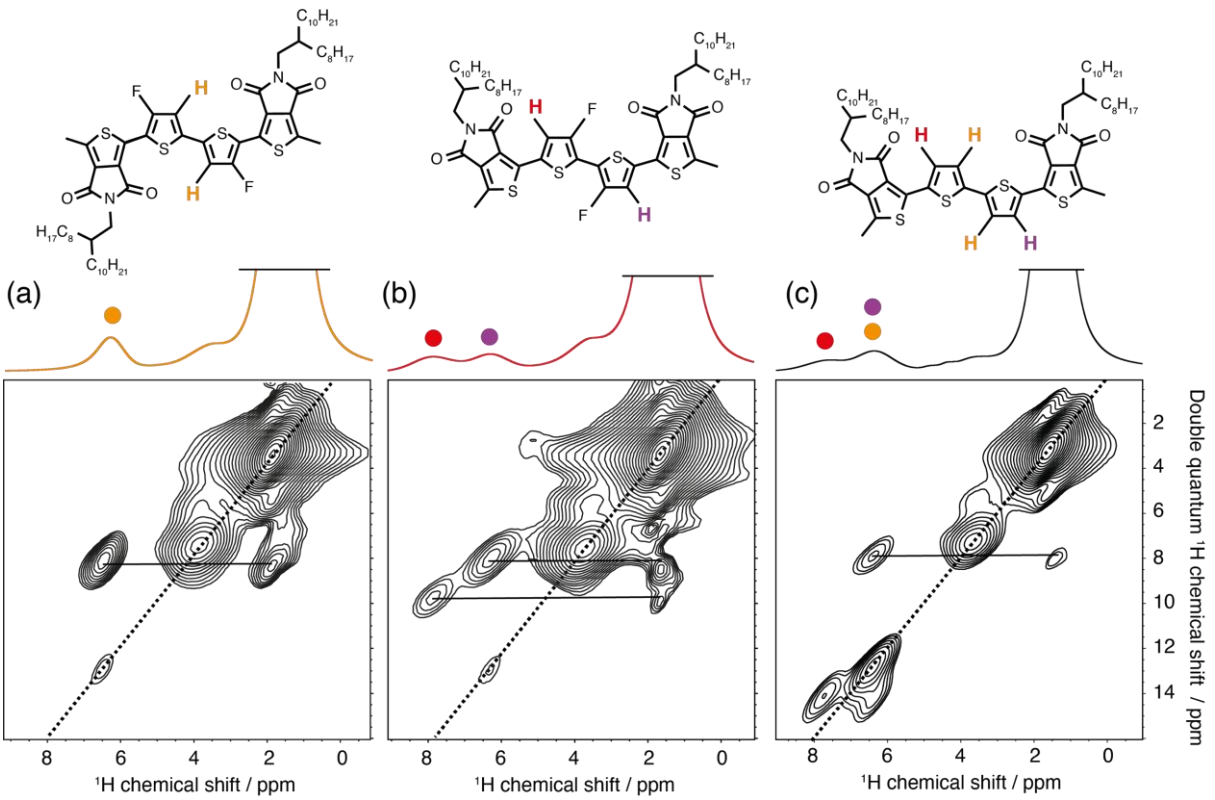

Figure 6. ^{1}H DQ-SQ MAS NMR spectra of the two fluorinated and the non-halogenated polymers: (a) P(TPD)-4FBT, (b) P(TPD)-3FBT, and (c) P(TPD)-BT, respectively. The spectra were recorded at 18.8 T with MAS frequency of 60 kHz, using the BABA pulse sequence[47] using a recoupling time of two rotor periods. The 1D spectra are displayed above the 2D plots. The schematic structure of the repeat units showing the labeling scheme for peak assignment are also reported. The dotted line in the 2D spectra represents the $\omega_1=2\omega_2$ diagonal.

The DQ-SQ experiment yields two-dimensional plot with (ω_1, ω_2) correlations between pairs of dipolar coupled (i.e., spatially close) protons. The DQ frequency in the indirect ω_1 dimension corresponds to the sum of the two single-quantum (SQ) frequencies of the two coupled protons and correlates in the ω_2 dimension with the two individual proton resonances. Thus, the observation of a DQ peak implies a close proximity between the two protons in question. In particular, two equivalent protons (or two protons having the same chemical shifts) give rise to correlation peak located along the $\omega_1 = 2\omega_2$ diagonal line of the 2D spectrum.

All the proton DQ-SQ spectra exhibit intense correlations along the diagonal at (ω_2, ω_1)=(1.6 ppm, 3.2 ppm) and (ω_2, ω_1)=(3.6 ppm, 7.2 ppm) corresponding to interactions among aliphatic protons of the polymer side chains. Correlations are also observed between the aromatic protons of the thiophene units and the aliphatic protons of the side chains, indicated by horizontal lines. More interesting are the correlations in the aromatic region of the spectra.

The DQ-SQ spectrum of **P(TPD-4FBT)** (Figure 6a) displays only a weak correlation at (ω_2, ω_1)=(6.4 ppm, 12.8 ppm) that corresponds to relatively long-range pairwise proximities between protons in 3,3' positions. This suggests that, in this polymer, the two protons of the 4,4'-difluorinated bithiophene unit are in a *trans* configuration from each other, the weak correlation observed along the diagonal stemming from intermolecular dipolar interactions between stacked polymer chain lamellae.

No correlation peak is observed between the two ^{1}H resonances at 6.4 and 7.9 ppm of **P(TPD-3FBT)** (Figure 6b). This is expected as these two protons are not spatially close. Only a weak autocorrelation is observed between the protons facing the TPD sulfur atoms (in purple) that again, likely corresponds to intermolecular interactions between stacked polymer chains. At this stage, no information can be deduced regarding the relative orientation of consecutive thiophene rings in adjacent TPD-thiophene units in **P(TPD-4FBT)**, nor in bithiophene units in **P(TPD-3FBT)**. Fortunately, fluorine atoms are very good NMR probes. Therefore, we recorded the ^{19}F NMR spectra of these two fluorinated polymers.

Figure 4b shows the 1D ^{19}F NMR spectra. The ^{19}F NMR spectrum of **P(TPD-3FBT)** displays a single resonance at -120.3 ppm. The ^{19}F DQ-SQ correlation experiment recorded over an experimental time of 36 hours does not show any autocorrelation, which suggests that consecutive thiophene cycles in the bithiophene unit of **P(TPD-3FBT)** are in a *trans* conformation, as depicted in the scheme of Figure 6b.

The ^{19}F spectrum of **P(TPD-4FBT)** shows a single resonance at -113.9 ppm, suggesting that the fluorine atoms all have the same local environment (Figure 4b). It appears at a higher chemical shift values that the one observed for the **P(TPD-3FBT**) polymer. DFT calculations of chemical shifts of fluorine atoms in 4,4'-positions show that both conformations lead to very similar and deshielded signals, as compared to the 3,3'-series (Figure 5) and therefore the ^{19}F NMR experiment does not allow to discriminate between the two possible adjacent TPD-Thiophene conformations. The shift between the **P(TPD-3FBT**) and **P(TPD-4FBT**), ca. 6 ppm is

consistent with the measurements. However, the DFT calculations give a significant information in the form of the difference in relative free energy of the two possible conformations (see Table 2 and previous discussion). It appears clearly that the *cis-trans* conformation is very unstable as compared to the *trans-trans* conformation. Consequently, we can consider that the **P(TPD-4FBT)** conformation is likely the *trans-trans* conformation.

The proton-proton DQ-SQ correlation spectrum of the **P(TPD-BT)** polymer shows two types of correlations in the aromatic region: a correlation peak along the diagonal for the 6.4 ppm resonance at around (ω_2, ω_1)=(6.4 ppm, 12.8 ppm) as well as correlations between the 6.4 and 7.9 ppm resonances (ω_2, ω_1)=(6.4 ppm, 14.3 ppm) and (ω_2,ω_1)=(7.9 ppm, 14.3 ppm). The later correlations are expected and reflect intra-ring interaction between protons of thiophene units in *cis* conformation with respect to the adjacent TPD group (*i.e., proximities* of "red" and "orange' protons in the scheme of Figure 6c). Similarly, proximity between protons in backbone thiophene units in *trans* conformation with respect to the adjacent TPD group (pair of "purple" and "orange" protons) will contribute to the diagonal correlation peak at (6.4 ppm, 12.8 ppm). In the scheme of Figure 6c, the bithiophene unit is represented with a trans conformation. However, a *cis* conformation could also be envisaged. In this case, the spatial proximity of the two inner protons (the "orange" ones) would also contribute to the intensity of the correlation peak along the $\omega_1 = 2\omega_2$ diagonal line. A close examination of the spectrum shows that the sum of the integrated intensity of the off-diagonal correlations at (ω_2,ω_1)=(7.9 ppm, 14.3 ppm) is significantly lower than the one of the correlation along the diagonal, by a roughly a factor 1.8. If the bithiophene units were all in a *trans* conformations, an intensity ratio of approximately 0.9 would be expected considering a *cis* to *trans* ratio of about 70/30 for the relative orientation of the TPD and backbone thiophene units, as deduced from the 1D spectra. While extracting truly quantitative information from the intensity of dipolar-based correlations is difficult, these numbers suggest that a significant fraction of the backbone thiophene units adopt a *cis* conformation, in which the two protons in 3 and 3' are spatially close and will contribute to the (ω_2,ω_1)=(6.4 ppm, 12.8 ppm) diagonal correlation.

The conclusions that could be derived for 1D and 2D ^{19}F and ^{1}H MAS NMR spectroscopy are summarized below and in the Figure 7.

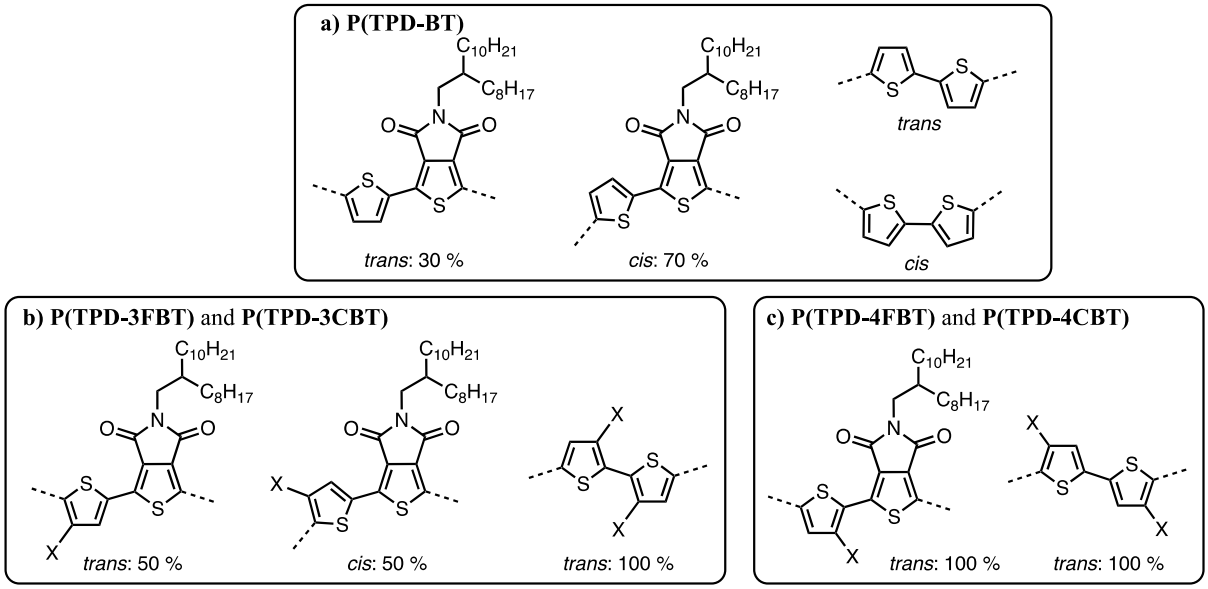

Figure 7. Summary of the possible conformations for each polymer, as extracted from the NMR data.

For the non-halogenated polymer, ***P(TPD-BT)****:* The conjugated backbone has several conformations (Figure 7a). The one-dimensional proton NMR spectrum showed that TPD-thiophene sequences adopt both *trans* and *cis* conformation in a 30 to 70 % ratio. The two-dimensional DQ-SQ correlation spectrum suggests that within the bithiophene unit both trans and cis conformation are present.

For the 3,3'-dihalogenated polymer ***P(TPD-3CBT)*** *and* ***P(TPD-3FBT)****:* The conjugated backbone exhibits fewer conformations (see Figure 7b) as the ^{19}F NMR showed that the bithiophene unit exhibits a pure *trans* conformation in **P(TPD-3FBT)**. 1D proton spectra indicated that in both polymers, the TPD-thiophene sequence adopts trans and cis conformations in a 50/50 ratio. From the 1D ^{1}H NMR spectrum recorded for the **P(TPD-3CBT)** (Figure S15), we assume that the conformation of the bithiophene unit is similar for the chlorinated polymer.

For the 4,4'-dihalogenated polymers ***P(TPD-4CBT)*** *and* ***P(TPD-4FBT)***: For these two polymers, the whole conjugated backbone exhibits only one possible *trans-trans* conformation (see Figure 7c). Indeed, the 2D proton spectra indicated that the bithiophene unit adopts *trans* conformation, while the ^{19}F spectrum, combined with DFT calculations, of **P(TPD-4FBT)** suggest that the TPD-thiophene sequence is in *trans* conformation too. Assuming this later is

also valid for the chlorinated polymer, a single structure is derived for the polymers halogenated in 4,4' positions.

SWAXS on powder analysis

Further, the polymer powders were characterized by SWAXS. The SWAXS patterns evidenced for the five polymers a mesophase organization with a smectic-like structure consisting in the alternation of stacked backbone and molten chains layers (Figures 8 and S15). This structure is frozen in solid state at room temperature and is kept at 180°C, after softening to paste-like mesophase. Further heating obviously preserves the same mesophase up to polymer decomposition since no phase transition was observed by polarized optical microscopy (POM) and DSC (Figures S5-S6). All patterns are characterized by a very intense π-stacking peak h_π irrespective of the halogen nature and position, and temperature. This feature is rather uncommon among halogenated organic semiconductor polymers. For example, our group has previously worked on a series of D/A alternating polymers using halogenated benzothiadiazole (substituted once or twice with fluorine or chlorine) as the electron-withdrawing unit, and alkylated thiophenes as the solubilizing electron-donating unit. While fluorine substituents were found to stabilize the lamellar organization, the chlorine substituents showed a drastic reduction of h_π and an early collapse of structure by heating.[26] In comparison with these previous polymers, the alkyl chains and halogens are here placed in opposite units, so that the bulky alkyl chains are now substituted on the protruding acceptor unit. This deeply modifies steric constrains from substituent bulkiness and the dipolar interactions between repeat unit rings, with the final outcome that the halogen nature has less significant impact on self-assembly. In contrast, the lamellar configuration is strongly influenced by the halogen position, as revealed by the smaller periodicity and the enhanced higher order reflections of 4,4'-dihalogenated polymers, compared to 3,3'-dihalogenated and to unsubstituted polymers giving close patterns.

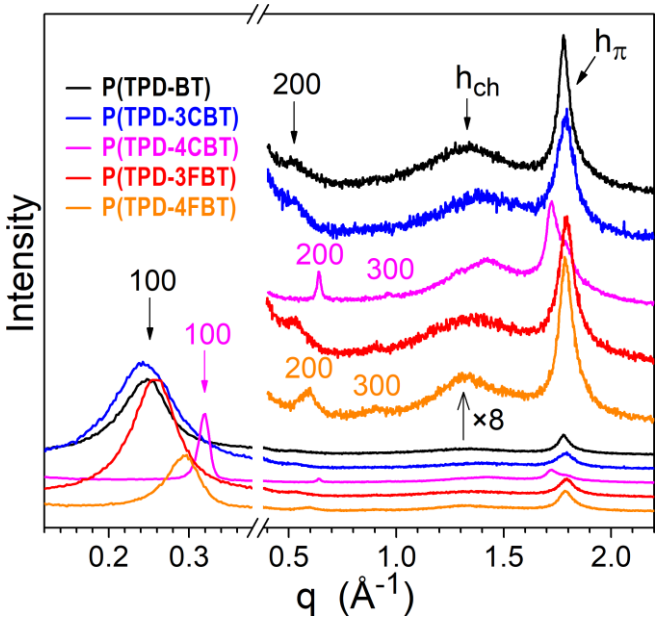

Figure 8. SWAXS patterns of the solid state of the polymer series at 20°C showing several reflections from lamellar periodicity (*h*00), the broad scattering signal from molten chain packing h_{ch} and the peak from backbone stacking h_{π}. Polymers **P(TPD-BT)**, **P(TPD-3CBT)** and **P(TPD-3FBT)** initially showed unique, broad lamellar reflection (Figure S16) and were preheated at 180°C to develop the structure to long range.

The information of patterns combined with calculated repeat unit volume V_{ru} allows specifying the features of the self-assembly (Table 3). The ratio of V_{ru} and lamellar periodicity d_{lam} determine the layer portion occupied by repeat unit, i.e., the repeat unit area A_{ru}, which lies around 34 Å^2 for **P(TPD-BT)** and 35-36 Å^2 for **P(TPD-3CBT)** and **P(TPD-3FBT)** (respectively, 35 Å^2 and 36-37 Å^2 at 180°C). These values are roughly 20% below the natural cross-section area of ramified alkyl side chains ($\sigma_{ch} \approx 43$ Å^2 at 20°C, ≈ 48 Å^2 at 180°C) and imply that the alkyl chains reduce their space-requirement by forming double-layers.[48] However, this configuration doubles the area per chain to values exceeding σ_{ch} by factor q_{ch} = 1.6-1.7 at room temperature and 1.5-1.6 at 180°C. Therefore, chains adopt slightly stretched conformations that promote irregular layer interfaces and partly explain the few higher-order reflections and the low correlation length of the layering. **P(TPD-4CBT)** and **P(TPD-4FBT)** show respectively 23% and 12% lower d_{lam} as their 3,3'-dihalogenated counterparts (12% and 9%, at 180°C), rising A_{ru} to value above σ_{ch} in the chlorinated polymer. Such lateral expansion allows the switching to alkyl monolayers with q_{ch} close to unity in **P(TPD-4CBT)**, meaning that chains from opposite lamellae stretch and intercalate.

Such configuration is associated to flatter and sharper layer interfaces explaining the increased lamellar correlation length and the enhanced higher-order reflections. On heating to 180°C, σ_{ch} expands above A_{ru} and chains disentangle into high-q_{ch} double-layers equivalent to those of the other polymers. Regarding the self-assembly of the backbones, all polymers show close π-stacking distances around 3.5 Å at 20°C and 3.6 Å at 180°C, with only slight deviation to 3.65 Å for the configuration with intercalated alkyl chains. The correlation length of the stacking ranges from 60 to 120 Å, representing 16 to 32 polymer backbone stacks.

Table 3. Self-assembly parameters of polymers at 20°C and 180°C.

	T[a] (°C)	V_{ru} [ρ][b] (Å^3)	d_{lam} [ξ][c] (Å)	A_{ru}[d] (Å^2)	$n_{L,ch}$[e]	q_{ch}[f]	h_π (ξ)[g] (Å)
P(TPD-BT)	20	855 [1.16]	25.34 [90]	33.7	2	1.59	3.53 [90]
	180	930 [1.06]	26.54 [90]	35.0	2	1.47	3.62 [80]
P(TPD-3CBT)	20	897 [1.23]	25.56 [60]	35.1	2	1.65	3.51 [60]
	180	973 [1.13]	26.87 [70]	36.2	2	1.52	3.60 [50]
P(TPD-4CBT)	20	897 [1.23]	19.69 [450]	46.6	1	1.07	3.65 [120]
	180	973 [1.13]	23.52 [120]	41.4	2	1.74	3.57 [80]
P(TPD-3FBT)	20	866 [1.21]	24.36 [80]	35.6	2	1.68	3.50 [60]
	180	941 [1.11]	25.75 [90]	36.6	2	1.54	3.59 [60]
P(TPD-4FBT)	20	866 [1.21]	21.38[120]	40.5	2	1.91	3.51 [70]
	180	941 [1.11]	23.43 [160]	40.2	2	1.69	3.59 [80]

[a] T: temperature; [b] V_{ru}, ρ: calculated repeat unit volume and density in g/cm^3; [c] d_{lam}, ξ: lamellar periodicity from (100) reflection and associated correlation length from peak width and Scherrer equation with shape factor K = 0.9; [d] A_{ru}: repeat unit area; [e] $n_{L,ch}$: number of chain layers per lamella; [f] $q_{ch} = \sigma_{ch}/A_{ru}$: chain packing ratio, $\sigma_{ch} = 42.5\ (1 + 7.5\times10^{-4}\ (T - 20))$ (Å^2) is the cross-sectional area, or molten, branched chain; [g] h_π, ξ: stacking distance from peak position and correlation length from peak width and Scherrer equation with shape factor K = 0.9.

The characteristics of polymer self-assembly are related to those of the backbone conformation that were investigated by solid-state NMR. Conformations were found to be strongly constrained by introduction of halogen atoms, with a strong dependence upon their position. **P(TPD-4CBT)** and **P(TPD-4FBT)** gave 100% *trans*-conformation of the TPD-thiophene sequence along with 100% *trans*-conformation of the bithiophene unit corresponding to antiparallel C-X bonds. The backbone conformation is hence identified to a syndiotactic-like sequence of repeat units that are aligned on chain axis with alternatively up and down oriented TPD (Figure 9). In **P(TPD-3CBT)** and **P(TPD-3FBT)**, TPD-thiophene sequence exhibits *cis* and *trans* conformations in similar proportions. Although the bithiophene units stay 100% antiparallel, the overall backbone conformation deviates from

linear sequence of aligned repeat units. The polymer tacticity is reduced as compared to **P(TPD-4XBT)** polymers. The suppression of the halogens in **P(TPD-BT)** further removes the constrains on thienyl ring orientations in bithiophene segments leading to both *cis* and *trans* conformations. In summary, **P(TPD-4CBT)** and **P(TPD-4FBT)** backbones stand out by their regular and fully-stretched conformation of periodicity: $D_{pol} = 2 \times L_{ru} = 23.2$ Å, whereas **P(TPD-3CBT)**, **P(TPD-3FBT**) and **P(TPD-BT)** adopt conformations that deviate from linear chain sequence and have reduced L_{ru} projection in lamellar plane.

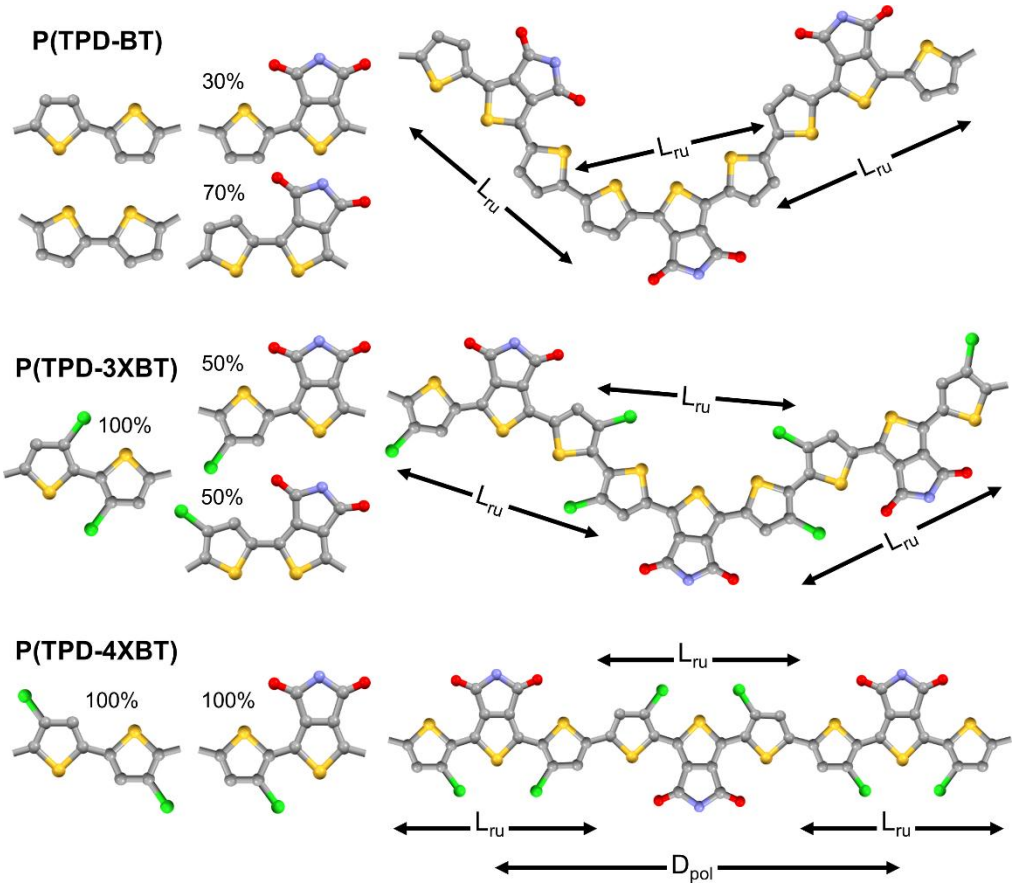

Figure 9. Model views of polymer backbone conformations, as deduced from NMR results and from single crystal structures of molecules with same segments, using Mercury and home-developed softwares. Left: proportions of segment conformations for polymers **P(TPD-BT)**, **P(TPD-3XBT)** and **P(TPD-4XBT)** (X = Cl, F). Right: example of **P(TPD-BT)** and **P(TPD-3XBT)** non-linear polymer segments (non-parallel repeat units of length L_{ru}); **P(TPD-4XBT)** conformation with aligned repeat units and backbone periodicity $D_{pol} = 2 \times L_{ru}$.

The knowledge of the conformation of backbones allows a deeper self-assembly analysis. For **P(TPD-4XBT)**, the projection of the repeat unit length in the lamellar plane is known to be $D_{ru} = D_{pol}/2 = 11.6$ Å, which in turn gives access to backbone spacing $h_{ru} = A_{ru}/D_{ru} = 3.9$ Å (**X** = Cl, 20°C), 3.6 Å (**X** = Cl, 180°C), 3.5 Å (**X** = F, 20°C), 3.6 Å (**X** = F, 180°C). For the self-assemblies with high-q_{ch} alkyl double-layers, h_{ru} and h_{π} values are in agreement, meaning that the lath-like backbones are π-stacked with their plane orthogonal to layers. For the low-q_{ch} monolayer case (**P(TPD-4CBT)** at 20°C), h_{ru} exceeds h_{π} by 8%, revealing that the backbones tilt or more probably fluctuate out of the layer plane to expand layers and allow side chain intercalation. The other polymers consist in a mixture of conformations that deviate significantly from straight lath-shape. The average deviation can be estimated from the ratio A_{ru}/h_{π} whose value is about 9.8 Å for both **P(TPD-3XBT)** polymers and 8.7 Å for **P(TPD-BT)**. These ratios are respectively 85 % and 75 % of the repeat unit length L_{ru} of the full stretched polymers **P(TPD-4XBT)**. Therefore, these polymers significantly deviate from linearity and thus also from planarity.

Charge transport properties

To characterize the charge transport properties of polymers, bottom–gate bottom–contact field effect transistors (FET) were fabricated following the procedure detailed in the SI. Hole and electron mobilities were both investigated after thermal annealing. The measured optimal mobilities are summarized in Table 4.

Table 4. Charge transport properties measured by OFET.

	Thermal annealing (min/T°C)	μ_h (cm^2/V.s)	μ_e (cm^2/V.s)
P(TPD-BT)	10 / 100	$(1.1 \pm 0.5) \times 10^{-4}$	$(4.5 \pm 1.6) \times 10^{-5}$
P(TPD-3CBT)	10 / 150	$(1.3 \pm 0.8) \times 10^{-4}$	$(7.8 \pm 4.2) \times 10^{-4}$
P(TPD-4CBT)	10 / 150	-	$(2.9 \pm 0.5) \times 10^{-5}$
P(TPD-3FBT)	10 / 150	$(2.1 \pm 1.0) \times 10^{-3}$	$(2.8 \pm 0.8) \times 10^{-3}$
P(TPD-4FBT)	10 / 150	-	$(1.2 \pm 0.2) \times 10^{-4}$

Interestingly, most of the polymers exhibit ambipolar charge transport properties. However, the two 4,4'-dihalogenated polymers only transport electrons. This could be due to deeper

HOMO levels which lead to significant energy barriers for the injection of holes. The structural information obtained from the combination of SWAXS and MAS-NMR on the full polymer series, helps to rationalize the UV-vis absorption observations and the charge transport properties as well.

Indeed, with four different conformations, it can be assumed that **P(TPD-BT)** is weakly ordered in the solid state, as illustrated by the very weak vibronic structure observed in thin-film UV-vis absorption and the poor charge transport mobilities as well.

Thanks to the intramolecular conformational locks (mainly sulphur-halogen weak bonds), the dihalogenated polymers exhibit fewer possible conformations. Amazingly, despite being the most constrained and linear materials within the series, with all segments locked in a pure *trans* conformation, **P(TPD-4CBT)** and **P(TPD-4FBT)**, exhibit lowest mobility values than their 3,3'-counterparts. In the specific case of **P(TPD-4CBT)**, the very low electron mobility measured is probably the consequence of the monolayer configuration adopted by this polymer at room temperature. To reach the space requirement imposed by the interdigitated side chains, the backbones must tilt out of the plane of the layers and slightly increase their stacking distance, which naturally impairs the efficiency of conduction pathways. For **P(TPD-4FBT)**, although it is difficult to provide definitive arguments, it can be noted that its lowest charge transport is consistent with a lower π-delocalization measured by UV absorption, compared to that of the **P(TPD-3FBT)** derivative. This lowest delocalization was further confirmed by DFT calculations with a less planar conjugated backbone and a blue-shifted absorption (Table 2) which should probably have an impact on the overlap of intra- and inter-molecular frontier orbitals. Furthermore, although in a fully stretched conformation, it can be envisaged that the way in which the backbones stack up is actually not conducive to efficient charge transport. Finally, the 3,3'-dihalogenated polymers, **P(TPD-3CBT)** and **P(TPD-3FBT)**, exhibit two possible conformations, with a possible rotation around the TPD-Thiophene bond. Nevertheless, these are the polymers in the series that show the highest electron delocalization and the highest charge mobilities. The chlorinated polymer, however, has significantly lower mobilities than its fluorinated counterparts probably due to sterically-induced side effect, as illustrated by the high twist angle measured for the bithiophene (ca 126.8°) by DFT for the *cis*-*trans* conformer.

Conclusion

Halogenation of organic semiconductor materials is probably one of the most commonly used chemical engineering approaches to adjust the optoelectronic and structural properties of conjugated materials. If a certain number of parameters are already well understood and established, their impact on the structure at the atomic scale is much less reported. Due to complex and sometimes contradictory impacts (steric hindrance, electrostatic interactions ...) and the lack of analytical tools to characterize the fine structure of polymers in particular, the conformational impact of halogen atoms on the conjugated backbone is most often suggested. In this study, we used the solid-state NMR spectroscopy under MAS to investigate the chemical bonds conformation, revealing the role of halogen nature and position on conjugated backbone conformational locking. In order to carry out a comprehensive study, we have first synthesized 5 polymers derived from the same family consisting of an alternation of a TPD unit and a bithiophene unit, either naked or dihalogenated. For this purpose, meanwhile, we have reconsidered the chemistry of dihalogenated bithiophenes and have synthesized a new 4,4'-dichloro-2,2'-bithiophene derivative never reported before.

Combined with DFT and TD-DFT calculations and SWAXS experiments, MAS NMR revealed that the position and, to a lesser extent, the nature of the halogens, had a profound impact on the free rotation of the chemical bonds between the aromatic units and thus the final conformation of the polymer chains. Thus, while all conformations are possible in the repeating unit when it is non-halogenated, the dihalogenation carried out at the 4 and 4' positions (presence of non-bonding interactions between sulphur and halogen atoms and sulphur and hydrogen atoms) results in only one fully *trans* conformation of this unit. In between, the 3,3'-dihalogenation offers a possible free rotation between the TPD unit and the bithiophene, resulting to two possible conformations for the repeating unit. However, counter-intuitively, the 4,4'-dihalogenated derivatives, although the most conformationally locked, are not the ones that present the best charge transport properties.

Beyond the results and measurements specific to this family of materials, this study demonstrates that solid-state NMR spectroscopy under MAS is a powerful tool, complementary to more conventional methods, to clarify in great detail the fine structural conformations of complex conjugated polymers.

Acknowledgments

Financial support from INAFRANALYTICS (FR2054 CNRS) for conducting the research is gratefully acknowledged.

References

[1] N. Leclerc, P. Chávez, O. Ibraikulov, T. Heiser, P. Lévêque, *Polymers* **2016**, *8*, 11.

[2] F. Meyer, *Prog. Polym. Sci*. **2015**, *47*, 70.

[3] C. Sun, S. Qin, R. Wang, S. Chen, F. Pan, B. Qiu, Z. Shang, L. Meng, C. Zhang, M. Xiao, C. Yang, and Y. Li, *J. Am. Chem. Soc.* **2020**, *142*, 3, 1465.

[4] O. A. Ibraikulov, B. Heinrich, P. Chávez, I. Bulut, C. Ngov, O. Boyron, N. Brouckaert, S. Swaraj, K. L. Gerasimov, D. A. Ivanov, S. Méry, N. Leclerc, P. Lévêque, T. Heiser, *J. Mater. Chem. A* **2018**, *6*, 12038.

[5] J. H. Park, E. H. Jung, J. W. Jung, W. H. Jo, *Adv. Mater.* **2013**, *25*, 2583.

[6] C. J. Mueller, E. Gann, C. R. McNeill, M. Thelakkat, *J. Mater. Chem. C* **2015**, *3*, 8916.

[7] Y. Cui, H. Yao, J. Zhang, T. Zhang, Y. Wang, L. Hong, K. Xian, B. Xu, S. Zhang, J. Peng, Z. Wei, F. Gao, J. Hou, *Nature Comm.* **2019,** 10:2515.

[8] G. Cavallo, P. Metrangolo, R. Milani, T. Pilati, A. Priimägi, G. Resnati, G. Terraneo, *Chem. Rev*. **2016**, *116*, 4, 2478.

[9] C. Dalvit, C. Invernizzi, A. Vulpetti, *Chem. Eur. J*., **2014**, 20, 11058.

[10] Z. Fei, P. Boufflet, S. Wood, J. Wade, J. Moriarty, E. Gann, E. L. Ratcliff, C. R. McNeill, H. Sirringhaus, J.-S. Kim, M. Heeney, *J. Am. Chem. Soc.* **2015**, *137*, 6866.

[11] J. E. Coughlin, A. Zhugayevych, R. C. Bakus II, T. S. van der Poll, G. C. Welch, S. J. Teat, G. C. Bazan, S. Tretiak, *J. Phys. Chem. C* **2014**, *118* (29), 15610.

[12] P. Boufflet, Y. Han, Z. Fei, N. D. Treat, R. Li, D.-M. Smilgies, N. Stingelin, T. D. Anthopoulos, M. Heeney, *Adv. Funct. Mater*. **2015**, *25*, 7038.

[13] H. Huang, L. Yang, A. Facchetti, T. J. Marks, *Chem. Rev.* **2017**, *117*, 15, 10291.

[14] T. Bura, S. Beaupré, O. A. Ibraikulov, M.-A. Légaré, J. Quinn, P. Lévêque, T. Heiser, Y. Li, N. Leclerc, M. Leclerc, *Macromolecules* **2017**, *50*, 7080.

[15] Y. Gao, Y. Deng, H. Tian, J. Zhang, D. Yan, Y. Geng, F. Wang, *Adv. Mater.* **2017**, *29*, 1606217.

[16] L. Shi, Y. Guo, W. Hu, Y. Liu, *Mater. Chem. Front*. **2017**, *1*, 2423.

[17] Q. Zhang, M. A. Kelly, N. Bauer, W. You, *Acc. Chem. Res*. **2017**, *50*, 2401.

[18] S. Xiao, Q. Zhang, W. You, *Adv. Mater*. **2017**, *29*, 1601391.

[19] X. Ma, Q. An, O. A. Ibraikulov, P. Lévêque, T. Heiser, N. Leclerc, X. Zhang, F. Zhang, *J. Mater. Chem. A*, **2020**, *8,* 1265.

[20] Z. Fei, F. D. Eisner, X. Jiao, M. Azzouzi, J. A. Röhr, Y. Han, M. Shahid, A. S. R. Chesman, C. D. Easton, C. R. McNeill, T. D. Anthopoulos, J. Nelson, M. Heeney, *Adv. Mater*. **2018**, *30*, 1705209.

[21] Y. Cui, Y. Xu, H. Yao, P. Bi, L. Hong, J. Zhang, Y. Zu, T. Zhang, J. Qin, J. Ren, Z. Chen, C. He, X. Hao, Z. Wei, J. Hou, *Adv. Mater*., **2021**, *33*, 2102420.

[22] T. J. Aldrich, M. Matta, W. Zhu, S. M. Swick, C. L. Stern, G. C. Schatz, A. Facchetti, F. S. Melkonyan, T. J. Marks, *J. Am. Chem. Soc*. **2019**, *141*, 3274.

[23] J. Yuan, Y. Zhang, L. Zhou, G. Zhang, H. L. Yip, T. K. Lau, X. Lu, C. Zhu, H. Peng, P. A. Johnson, M. Leclerc, Y. Cao, J. Ulanski, Y. Li, Y. Zou, *Joule*, **2019**, *3*: 1140.

[24] Y. Wu, Y. Zheng, H. Yang, C. Sun, Y. Dong, C. Cui, H. Yan, Y. Li, *Sci. China Chem.*, **2019**, 62.

[25] Y. Cai, Y. Li, R. Wang, H. Wu, Z. Chen, J. Zhang, Z. Ma, X. Hao, Y. Zhao, C. Zhang, F. Huang, Y. Sun, *Adv. Mater*., **2021**, *33*, 2101733.

[26] T. Olla, O. A. Ibraikulov, S. Ferry, O. Boyron, S. Méry, B. Heinrich, T. Heiser, P. Lévêque, N. Leclerc, *Macromolecules*, **2019**, 52, 21, 8006-8016.

[27] J. Rivnay, M. F. Toney, Y. Zheng, I. V. Kauvar, Z. Chen, V. Wagner, A. Facchetti, A. Salleo, *Adv. Mater*., **2010**, *22*, 4359.

[28] D. Dudenko, A. Kiersnowski, J. Shu, W. Pisula, D. Sebastiani, H. W. Spiess, M. R. Hansen, *Angew. Chem. Int. Ed*., **2012**, *51*, 11068.

[29] H. N. Tsao, D. M. Cho, I. Park, M. R. Hansen, A. Mavrinskiy, D. Y. Yoon, R. Graf, W. Pisula, H. W. Spiess, K. Müllen, *J. Am. Chem. Soc*., **2011**, *133*, 2605.

[30] R. Stalder, S. R. Puniredd, M. R. Hansen, U. Koldemir, C. Grand, W. Zajaczkowski, K. Müllen, W. Pisula, J. R. Reynolds, *Chem. Mater.*, **2016**, *28*, 1286.

[31] K. R. Graham, C. Cabanetos, J. P. Jahnke, M. N. Idso, A. El Labban, G. O. Ngongang Ndjawa, T. Heumueller, Koen Vandewal, A. Salleo, B. F. Chmelka, A. Amassian, P. M. Beaujuge, M. D. McGehee, *J. Am. Chem. Soc*., **2014**, *136*, 27, 9608.

[32] A. Karki, G.-J. A. H. Wetzelaer, G. N. M. Reddy, V. Nádaždy, M. Seifrid, F. Schauer, G. C. Bazan, B. F. Chmelka, P. W. M. Blom, T.-Q. Nguyen, *Adv. Funct. Mater*., **2019**, *29*, 1901109.

[33] S. R. Chaudhari, J. M. Griffin, K. Broch, A. Lesage, V. Lemaur, D. Dudenko, Y. Olivier, H. Sirringhaus, L. Emsley, C. P. Grey, *Chem. Sci.* **2017**, *8*, 3126.

[34] H. Huang, L. Yang, A. Facchetti, T. J. Marks, *Chem. Rev.*, **2017**, *117*, 10291.

[35] M. Saito, T. Fukuhara, S. Kamimura, H. Ichikawa, H. Yoshida, T. Koganezawa, Y. Ie, Y. Tamai, H. D. Kim, H. Ohkita, I. Osaka, *Adv. Energy Mater*., **2020**, *10*, 1903278.

[36] K. Wang, Z. Xu, B. Guo, X. Guo, M. Zhang, Y. Li, *RSC Adv*., **2016**, 6, 63338.

[37] G.-S. Ryu, Z. Chen, H. Usta, Y.Y. Noh, A. Facchetti, *MRS Communications*, **2016**, *6*(01), 47.

[38] J. W. Jo, J. W. Jung, H.-W. Wang, P. Kim, T. P. Russell, W. H. Jo, *Chem. Mater*., **2014**, *26* (14), 4214.

[39] K. Kawashima, T. Fukuhara, Y. Suda, Y. Suzuki, T. Koganezawa, H. Yoshida, H. Ohkita, I. Osaka, K. Takimiya, *J. Am. Chem. Soc.,* **2016**, *138* (32), 10265.

[40] M. Kim, W.-T. Park, S. A. Park, C. W. Park, S. U. Ryu, D. H. Lee, Y.-Y. Noh, T. Park, *Adv. Funct. Mater*., **2019**, *29*, 1805994.

[41] L. Biniek, C. L. Chochos, G. Hadziioannou, N. Leclerc, P. Lévêque, T. Heiser, *Macromol. Rapid Commun*., **2010**, *31*, 651.

[42] Y. Liu, J. Zhao, Z. Li, C. Mu, W. Ma, H. Hu, K. Jiang, H. Lin, H. Ade, H. Yan, *Nat. Commun*., **2014**, *5*, 5293.

[43] A. P. Kulkarni, C. J. Tonzola, A. Babel, S. A. Jenekhe, *Chem. Mater*., **2004**, *16*, 4556.

[44] D. Chen, Y. Zhao, C. Zhong, S. Gao, G. Yu, Y. Liu, J. Qin, *J. Mater. Chem.*, **2012**, *22*, 14639.

[45] J. W. Jung, T. P. Russell, W. H. Jo, *ACS Appl. Mater. Interfaces,* **2015**, *7*, 13666.

[46] J. Huang, L. Xie, L. Hong, L. Wu, Y. Han, T. Yan, J. Zhang, L. Zhu, Z. Wei, Z. Ge, *Mater. Chem. Front.*, **2019**, *3* (6), 1244.

[47] W. Sommer, J. Gottwald, D. E. Demco, H. W. Spiess, *J. Magn. Reson., Ser. A*, **1995**, *113*, 131.

[48] N. Kamatham, O. A. Ibraikulov, P. Durand, J. Wang, O. Boyron, B. Heinrich, T. Heiser, P. Lévêque, N. Leclerc, S. Méry, *Adv. Funct. Mater.,* **2021**, *31*, 2007734.

Table of Contents

Solid-state nuclear magnetic resonance (NMR) under magic angle spinning (MAS) has been used to investigate the local structure and supramolecular organization of conjugated polymers, specially designed for this study. Through a comprehensive study using complementary small and wide-angle X-ray scattering (SWAXS) and molecular modelling investigations, the molecular conformation of these polymers in relation to their chemical composition has been fully determined.